ORIGINAL ARTICLE

Brain states in freely behaving marmosets

Olga Bukhtiyarova[1,2], Sylvain Chauvette[2], Josée Seigneur[2] and
Igor Timofeev[1,2,*,○]

[1]Department of Psychiatry and Neuroscience, School of Medicine, Université Laval, Québec (Québec), Canada and
[2]CERVO Brain Research Centre, Québec (Québec), Canada

*Corresponding author. Igor Timofeev, Faculté de Médecine, Département de Psychiatrie et de Neurosciences, Centre de Recherche du CERVO, Université Laval, Québec, QC G1J2G3, Canada. Email: igor.timofeev@fmed.ulaval.ca.

Abstract

Study Objectives: We evaluated common marmosets as a perspective animal model to study human sleep and wake states.
Methods: Using wireless neurologger recordings, we performed longitudinal multichannel local field potential (LFP) cortical, hippocampal, neck muscle, and video recordings in three freely behaving marmosets. The brain states were formally identified using self-organizing maps.
Results: Marmosets were generally awake during the day with occasional 1–2 naps, and they slept during the night. Major electrographic patterns fall in five clearly distinguished categories: wakefulness, drowsiness, light and deep NREM sleep, and REM. Marmosets typically had 14–16 sleep cycles per night, with either gradually increasing or relatively low, but stable delta power within the cycle. Overall, the delta power decreased throughout the night sleep. Marmosets demonstrated prominent high amplitude somatosensory mu-rhythm (10–15 Hz), accompanied with neocortical ripples, and alternated with occipital alpha rhythm (10–15 Hz). NREM sleep was characterized with the presence of high amplitude slow waves, sleep spindles and ripples in neocortex, and sharp-wave-ripple complexes in CA1. Light and deep stages differed in levels of delta and sigma power and muscle tone. REM sleep was defined with low muscle tone and activated LFP with predominant beta-activity and rare spindle-like or mu-like events.
Conclusions: Multiple features of sleep–wake state distribution and electrographic patterns associated with behavioral states in marmosets closely match human states, although marmoset have shorter sleep cycles. This demonstrates that marmosets represent an excellent model to study origin of human electrographical rhythms and brain states.

Statement of Significance

Understanding normal sleep or sleep pathology in human requires animal models that closely match human sleep–wake patters and that enable experimental manipulations, including invasive techniques. Sleep–wake pattern in commonly used laboratory animals for sleep research contain many drawbacks. Here, we performed long-lasting recordings with intracranial electrodes in small new world monkey, marmosets. Like human, marmosets slept during dark phase and were awake during light phase of light–dark cycle, they had clearly identified sleep cycles and we identified five clear states: wake, drowsiness, light- and deep-NREM sleep, and REM sleep. Multiple electrographic features were similar to human: slow waves, spindles, beta bursts, hippocampal, and cortical ripples etc. We conclude that marmosets represent an excellent model of human brain states.

Introduction

All brain functions or pathological processes are executed in a given behavioral state. For example, although the learning occurs mostly during wake, memory consolidation primarily happens during sleep [1–3]. Epileptic seizure activities reveal strong interactions with sleep and wake behavioral states, and neocortical epilepsy is mostly nocturnal [4, 5].

Deep understanding of brain functions requires invasive methods of investigation, which are impossible in healthy humans. Commonly used laboratory animals for sleep research (rodents, carnivores) contain many drawbacks because of very fragmented sleep–wake states, sleeping during light phase of light–dark cycle (rodents) or being awake mainly at transitions between light cycles (carnivores), etc. [6–13].. This makes translational research problematic. Several studies on large nonhuman primates reported successful sleep–wake recordings [14–17]. These recordings were relatively short and often performed with some form of restraining or isolation of monkeys in individual cages, which could alter sleep–wake behavior. In addition, the life expectancy of large monkeys, such as macaques or baboons, spans for tens of years, and investigation of age-dependent changes of sleep and associated pathologies is unpractical in these animals.

Therefore, there is an emergent need to find an animal model suitable for translational research of sleep–wake cycle.

The overall objective of our study was to investigate sleep–wake cycle and accompanying brain activities in common marmosets. Common marmosets are New World monkeys with a small body weight, high speed of reproduction and relatively short lifespan in comparison to other primates, which make them suitable for studies of aging [18]. Their genome has been decoded, thus enabling development of effective genetic tools for brain research [19–21]. Marmosets were used as a model to study social cognition [22, 23]. All that makes marmosets a promising primate model for sleep research.

There were several previous studies on sleep–wake cycle in marmosets based on actigraphy [24] or bipolar EEG recordings [25–29]. These studies demonstrated that marmosets are diurnal animals and sleep mostly at night. However, there were differences in duration and number of episodes of each state of vigilance between the studies. It could be due to unclear definition of NREM sleep stages, location of recording electrodes and references, or particular features of animal husbandry such as size of the home cage or social and physical contacts with other animals.

A description of marmoset local field potential (LFP) sleep–wake cycle is lacking. The brain states detected with EEG may be incongruent to LFP states because EEG does not pick up regional differences in state expression [30–33]. Besides well accepted phenomenon of local sleep [34], there are evidences that in some cortical locations in mice [33, 35] and human [36], slow wave activity can be recorded during typical patterns of REM activity in other cortical regions.

Here, we performed longitudinal wireless multichannel LFP recordings from five neocortical areas: frontal, primary motor, primary somatosensory, associative parietal, and associative visual, as well as from ventral hippocampal CA1 in three freely behaving marmosets, that were housed in a group. We demonstrated the most common LFP patterns in five different brain states: wake, drowsiness, light and deep NREM sleep, and REM sleep. The results of our study demonstrate that marmosets represent an excellent animal model to study human sleep–wake activities as they are diurnal, they have monophasic sleep, they display light and deep stages of non-REM sleep, in addition to clear sleep electrographic events such as slow waves and spindles. The use of invasive methodology adds possibility to study regional differences in brain activities in particular, in a very high frequency (ripple) range.

Methods

All animal care procedures were conducted according to Canadian Guidelines for Animal Care and the specific research protocol was approved by Animal Care Committee of Université Laval.

Housing of marmosets

Three intact male marmosets were purchased at the age of about 1 year from Comparative Medicine and Animal Resources Center (CMARC) Breeding Colony (McGill University, Montreal, Qc, Canada), two of them (G and R) were twins. All three marmosets were housed in a single cage (2 m × 1 m × 2 m) with two metal mesh grid walls within a separate room. For environmental enrichment, the cage contained a hut, a hammock, wooden horizontal and vertical bars for climbing, and toys (such as hanging rings, small ladders, or rattles). The toys were replaced every 2 weeks. The marmosets usually chose to sleep in a hut or in a hammock located in the upper part of the cage. Marmosets were housed in 12 h/12 h light/dark regimen with lights off at 7 p.m. Each light/dark period was preceded by 30 min of dawn/dusk.

Marmoset diet

Food was provided ad libitum, fresh food was placed in different parts of the cage twice a day—at 7h30–8h30 and 14h00–14h30. Marmoset diet followed a weekly calendar that was regularly reviewed to provide environmental enrichment and to correspond to preferences of the animals. Typical weekly diet was as follows. Every morning: 1 bottle of water and 0.5 bottle of Gatorade drink (The Gatorade Company, Inc., Chicago, IL, USA); gum of acacia, 15 mL of Zupreem Marmoset Diet (Zupreem, Shawnee, KS, USA) mixed with 15 mL of DietGel Marmoset (ClearH$_2$O, Portland, ME, USA), 10 mL of hard-boiled egg. Daily rotation of fruits morning/afternoon, 0.25 cups each meal: Monday: blueberry/papaya, Tuesday: kiwi/papaya, Wednesday: grapes/pear, Thursday: pear/blueberry, Friday: papaya/kiwi, Saturday: pear/papaya, Sunday: pear/grapes. Cleaning of the cage, evaluation of animal appetite and digestion (feces) was performed daily during food placement.

Behavioral training

After habituation of the marmosets to the new facility, we started observation of normal marmoset behavior and training that would promote their handling after future surgery. The handling was needed to replace battery and memory card (see below). We attached three small birdcages (34 cm × 27.5 cm ×

45 cm) to the inner walls of the large home cage. The birdcages were modified to enable opening of the door by the experimenter from the outside of the large home cage. To reduce stress due to handling, marmosets were trained to enter the smaller cages to get a positive reinforcement in the form of a fruit, gum of acacia or a small piece of marshmallow. After closing the small cages, a technician entered the large cage and placed a custom-made curtain on a birdcage. When the door of the birdcage was open, the marmoset jumped out into the curtain and where they were captured by a technician. The animal received a reward from experimenter during handling.

Surgery

At time of the surgery the age of the animals was 34 (BB) and 32.5 (G and R) months old. The weight was 394 ± 19 g. Prior to the surgery the animals were withdrawn from food for at least 4–6 h. The premedication included ketamine (10–20 mg/kg) and buprenorphine (0.01 mg/kg). The temperature was maintained at 37°C. For intubation, the animals received spray of xylocaine 2% into larynx. During the entire surgery, the anesthesia was maintained with isoflurane 1%–3% and a Ringer's lactate solution (10 mL/kg/h, i.v.) was continuously injected. At the incision site and pressure points of the stereotaxic frame, lidocaine/marcaine (2 mg–5 mg/kg) was injected. The craniotomies were performed for placement of electrodes. Five stainless steel custom-made electrodes with Teflon insulation (125 μm diameter, wire from A-M systems, Sequim, USA) were implanted in the cortex and one tungsten electrode (10 MΩ) was implanted in hippocampus. Coordinates used for stereotaxic placements were based on Marmoset Brain Atlas [37] and confirmed location of the electrodes were evaluated on histological sections.

One more craniotomy was performed at coordinates AP +2 mm A, L 3 mm. A chamber containing a hidden custom-made knife was placed above dura mater and was used after the end of the current experiment to produce a brain trauma (not reported here).

Two stainless steel Teflon-insulated custom-made electrodes (75 μm diameter, wire from A-M systems, Sequim, WA, USA) were inserted in neck muscles for electromyography.

A silver wire was placed above cerebellum (AP -5 mm, L 2 mm) and used as a reference for monopolar recordings. All electrodes were soldered to Omnetics connector (Omnetics, Minneapolis, MN, USA).

For anchoring all implanted electrodes, eight screws were inserted in the cranium in the periphery of skin incision. The screws, craniotomies, and the electrodes were covered with dental acrylic (Dentsply-Canada), in which the Omnetics connector to the recording system and a plastic protector (upper part of 50 mL tube with cover lid) were integrated. The use of this protector prevented any manipulation of the neural logger by the marmosets, and we never observed an attempt of animals to manipulate with a protector.

Postsurgery treatment

After neurosurgery, the animals received meloxicam 0.2 mg/kg, Ringer's lactate solution (5–10 mL, s.c.). Meloxicam 0.1 mg/kg was given once a day up to 3 days following the surgery. During postsurgery recovery period that lasted from 8 to 15 days, marmosets were housed individually in a transport cage (0.6 m × 0.6

m × 1.2 m). During 5 days of postsurgery period, to facilitate the recovery, in addition to regular ad libitum diet, the marmosets received per os water, DietGel, Gatorade, suspension of gum of acacia and/or Ensure (Abbott Nutrition, Abbott, IL, USA), up to 5–7 mL of total volume twice a day. In post-surgery period, marmoset BB was diagnosed with abdominal distension and anorexia, and received Ranitidine 0.01 mL s.c. (25 mg/mL) on days 4-5, Cyproheptadine 0.2–0.3 mL s.c. (0.4 mg/mL) on days 12–15 twice a day, and Dexamethasone 0.4 mL i.m. (5 mg/mL) on days 15–18 in the morning.

All animals could hold their heads within the first day after surgery. During the entire experiment that lasted up to 7 months, the marmosets neither seemed to be disturbed by presence of implant nor tried to remove it or open the plastic protector.

Recordings

All the recordings reported in this study were done in the home cage in which marmosets spent more than one year prior to the beginning of experiment. The LFP and EMG recordings were started immediately after surgery with a light weight wireless MouseLog-8LP neural logger (Deuteron Technologies Ltd.) with bandpass filter 1–500 Hz. The sampling rate was 4 kHz.

For power supply, we used rechargeable Lithium-polymer flat batteries (400 mAh, 3.7 mV, 7 mm × 20 mm × 30 mm, Ultralast) that enabled continuous recordings during 17–32 h. To facilitate the battery replacement in awake animals, we used a single-row 2-pin male connector (A24002-002) wired to batteries that matched to a single-row 2-sockets female connector of the head stage (A25002-002) (Omnetics).

The data were stored in micro-SD memory card (Transcend Information, Ltd.). The memory card and the batteries were replaced daily (usually 4 continuous days per week).

Video recordings

Three night-vision cameras (DCS-5222L, D-Link, Taiwan) were installed around marmoset cage. If needed, the video recordings were synchronized with electrophysiological recordings.

Data analysis

Because postsurgery recovery and treatment could affect sleep–wake activities, we analyzed only data recorded after the end of recovery period. For the present study, we included in analysis 818 h of LFP recordings (385.5 from day time and 432.5 from night time).

All the data processing was done in MATLAB (MathWorks Inc., Natick, MA, USA), visual inspection of data and figures were done in IgorPro (WaveMetrics Inc., Lake Oswego, OR, USA) and Canvas Draw (Canvas GFX, Inc., Plantation, FL, USA).

With a custom-written code the data were exported to MATLAB and stored in files containing 1–2 h of continuous recordings for further data analysis. For LFP analysis of activities below 100 Hz, the data were downsampled to 1 kHz.

Filtering original signal. For illustration purposes we applied 80–300 Hz band pass filter for LFP high frequency oscillations (see Figure 2) and 50 Hz high pass filter to EMG (Butterworth, 3 order, zero-phase, Figures 1 and 2).
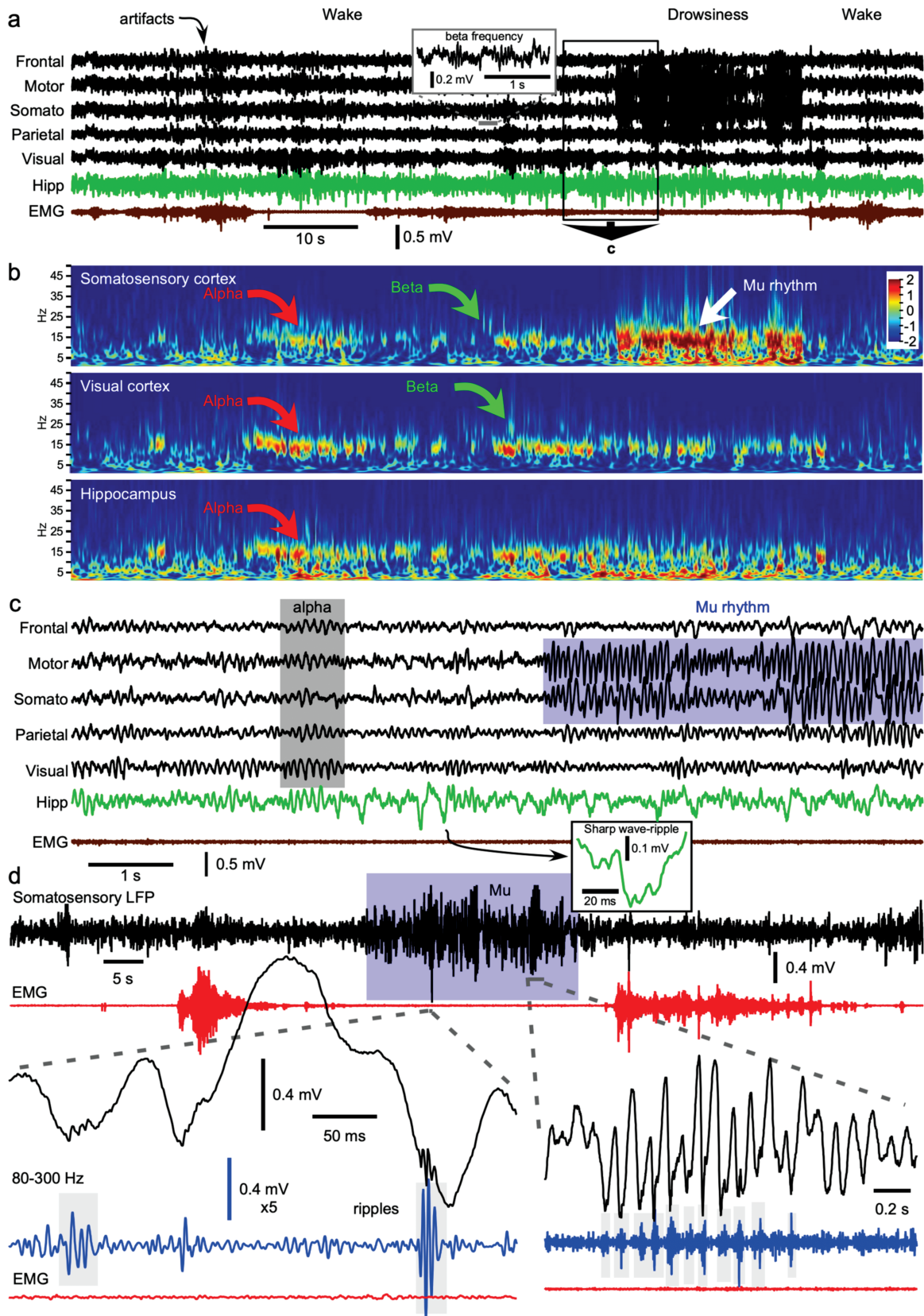
Figure 1. Multi-site LFP during waking states and drowsiness. **(a)** Original LFP from five cortical electrodes, CA1 area of hippocampus and EMG during wake and drowsiness. The insert shows an expanded segment of 2 s of LFP from somatosensory area with events in beta frequency range. The part of recordings included into a black box is expanded in panel c. **(b)** Time–frequency analysis with continuous wavelet transform corresponding to LFP recordings from somatosensory, visual and CA1 hippocampal areas from panel a. Red arrows point to Alpha rhythm, green arrows to Beta rhythm, and white arrow to Mu rhythm. **(c)** Expanded box from panel A that shows original LFP from all recorded sites and EMG. Arrow points to an expanded hippocampal ripple from a sharp wave-ripple complex. **(d)** Somatosensory Mu rhythm occur in the absence of movements (dramatic reduction of muscle tone) and it is accompanied with neocortical ripples.
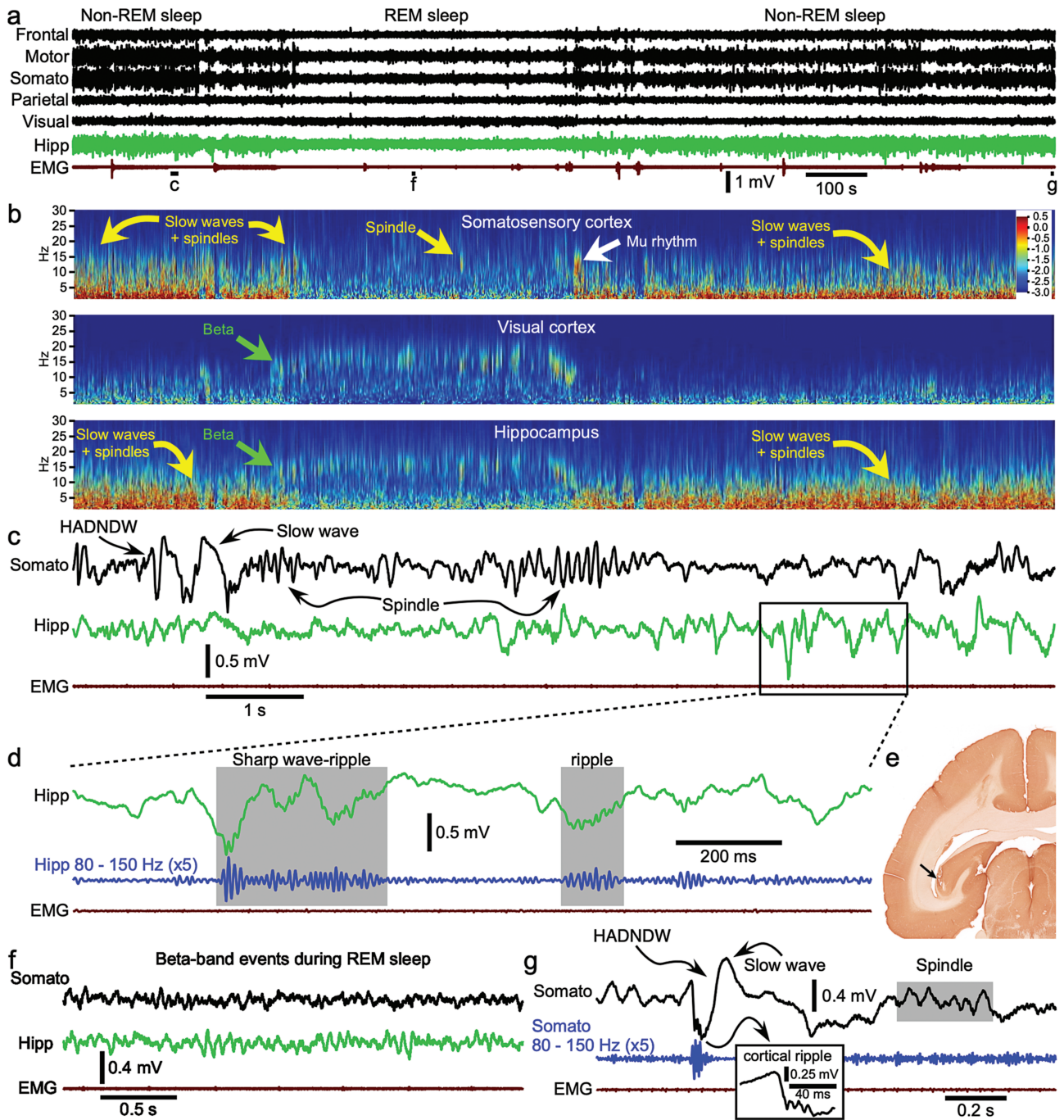
Figure 2. Multi-site LFP during sleep. (a) Original LFP from five cortical electrodes, CA1 area of hippocampus, and EMG during light NREM, deep NREM, and REM sleep as indicated. Horizontal lines with indications c, g and f and expanded in corresponding panels. (b) Time–frequency analysis with Continuous Wavelet Transform of recordings from somatosensory, visual and CA1 electrodes shown in panel a. Yellow arrows point to slow waves and sleep spindles frequencies during NREM sleep. Green arrows point to events in the beta frequency band during REM. White arrow in somatosensory panel points at brief mu-like activity at transition between REM and NREM sleep. (c) Expanded somatosensory, hippocampal LFPs and EMG from the box in panel a with examples of slow wave, sleep spindles, sharp-wave ripple, and isolated ripple. (d) Expanded hippocampal recordings with an example of sharp wave-ripple and an isolated ripple with corresponding filtered trace and EMG. (e) Trace of electrode placed in CA1 area of hippocampus from which the recordings demonstrated in Figures 1 and 2 were conducted. (f) Example of high-amplitude depth-negative delta wave (HADNDW), neocortical ripple, slow wave and a spindle recorded from somatosensory area during NREM sleep. (g) Example of activated LFP during REM sleep with events in beta band.

Wavelet decomposition for illustrations. We performed continuous wavelet transform (Morlet mother wavelet, s_0 0.02, ds 0.05, 114 scales) of original signal that was downsampled to 1 kHz to display LFP activities from 1 to 50 Hz (Figures 1 and 2).

Power analysis. We calculated LFP power in delta (1–4 Hz) and sigma (9–16 Hz or 12–16 Hz) frequency ranges, as well as muscle power (EMG, 50–300 Hz). During initial analysis we have chosen 5 s, 10 s, and 30 s windows. Because of high variability in rate of occurrence of slow waves in light and deep NREM sleep,

we chose 30 s sliding window for power calculations that was shifted every second (29 s overlap). This way we obtained power values corresponding to each second of the recordings that was based on the data within ±15 s from each time point.

Visual brain state detection. During visual examination of original LFP, we distinguished five different brain states. The results of visual sleep–wake scoring done by two independent observers were used as a golden standard to evaluate accuracy of automatic state detection. We defined wakefulness based on high muscle activity and activated LFP or alpha rhythm over visual cortex. Drowsiness was defined based on low stable muscle tone and presence of high amplitude rhythmic LFP activity in 9–16 Hz dominating in somatosensory and/or motor cortex. NREM sleep was defined based on presence of slow waves and spindles and stable or decreasing muscle tone. In long sleep episodes we could distinguish light and deep NREM based on amplitude and frequency of occurrence of slow waves and spindles and on stable or decreasing muscle tone. However, it was often difficult to discriminate visually the two states, that is why for comparison with automatic detection we combined two stages of NREM sleep in one. REM sleep was visually defined as a state with activated LFP and low stable muscle tone that started after drowsiness or NREM sleep. Brief interruptions of REM sleep shorter than 5 s (muscle jerks) were ignored, but occasionally muscle tone was increased for tens of seconds (see results).

Automatic brain state detection. We developed a procedure for automatic brain state detection with the use of artificial neural network—self-organizing map (see Figure 5). First step consisted of training of artificial neural network that was conducted separately for each marmoset. We used results of calculations of delta power, sigma power, and muscle power obtained from one continuous day–night recording. For brain state detection we chose somatosensory channel for marmosets BB and G as a channel that showed the highest delta power, displayed spindles and mu-rhythm. For marmoset R we used sum of these power bands calculated from three channels—primary motor, somatosensory and parietal. The input dataset for training consisted of three planes (for log-normalized delta, sigma, and muscle power) that contained data points corresponding to every second of the day–night recording (see Figure 5d, e). We used self-organizing map of hexagonal topology that consisted of 4 × 3 neurons to divide all the time points in 12 clusters. After the training, we combined several clusters to obtain five classes corresponding to each brain state (active wake, drowsiness, light NREM, deep NREM, and REM). The combining of the clusters was based on distances between the neurons, evaluation of weights from each plane and on visual inspection of the results of state detection in at least 1 full day of recordings from each animal. The results of automatic state detection were compared with manually scored hypnograms done by two independent experts from 1 hour of day and 1 hour of night recordings from each animal (6 h total).

As the result of the network training, for each animal, we obtained a neural network that was applied to other days of recordings of the same animal. We chose days after the end of postsurgery recovery that had stable distribution of these parameters throughout analyzed period. We included data from 12 days of B, 18 days of G and 4 days of marmoset R.

The procedure was followed by combining of clusters and determination of the beginning and the end of each state, their number, duration, time share spent in each hour, and pattern of transitions between brain states.

Detection of sleep cycles. To ignore brief fluctuations of delta power and short interruptions of sleep, continuous night delta power from somatosensory channel was smoothed with moving average 300 s windows. Based on visual examination, we established a threshold for obtained values equal to 0.002 that corresponded to low delta during wake or REM. We considered a sleep cycle as a time period between the beginning of drowsiness/NREM sleep to the end of the following consolidated REM or waking state. The onset of a sleep cycle was set when smoothed delta power exceeded the predefined threshold and the end of the sleep cycle was set at a time point prior to the beginning of the next cycle. To normalize duration of the sleep cycles, each of them was divided into 12 equal parts. If mean delta power of any part of the cycle was higher than mean delta power in the beginning of the cycle (the 1st part) at least 2.2 times, we considered this sleep cycle as "growing delta". Otherwise, it was considered as "stable delta" sleep cycle (see Figure 3).

After determining the type of the sleep cycle, each of them was divided in 240 equal bins, and mean delta and sigma power was calculated for each bin. Next, delta and sigma power from each normalized time period was averaged between all sleep cycles of this kind.

Results

Behavioral observations

Marmosets lived in a group of three animals and their behavior was not restricted except during changing of a battery and a memory card. During entire period of the study, we observed that their behavior was influenced by their social status in the group. During waking state, marmosets were primarily foraging for food, investigating toys or grooming. Marmosets G and B that originated from different families, displayed competitive behavior throughout the entire period of observation, that manifested in chasing one another, sometimes with biting, and competing for toys and treats. Their dominating status was not permanent, and it seemed to change every several weeks or months. Marmoset R mostly stayed away from this competition, that could indicate its submissive position; however, it received grooming more often from two other marmosets. The animals actively communicated with each other with sounds, and clearly warned their peers when a human was approaching. They displayed curiosity to familiar humans. Depending on their current dominating status, either marmoset G or B was the first to approach a human to receive a treat or to investigate a proposed toy, after a short while other animals also approached. Despite many hours the experimenter spent with the animals over several months, they did not allow to be touched and rapidly escaped when simple handling was attempted. With the use of a positive reinforcement (gum of acacia or piece of marshmallow proposed on a bamboo stick), they were trained to enter smaller cages that facilitated their handling.

Marmosets displayed a behavioral state that was transitory between wake and sleep. It was manifested with quiet behavior, brief periods of closed eyes and relaxing neck muscles,
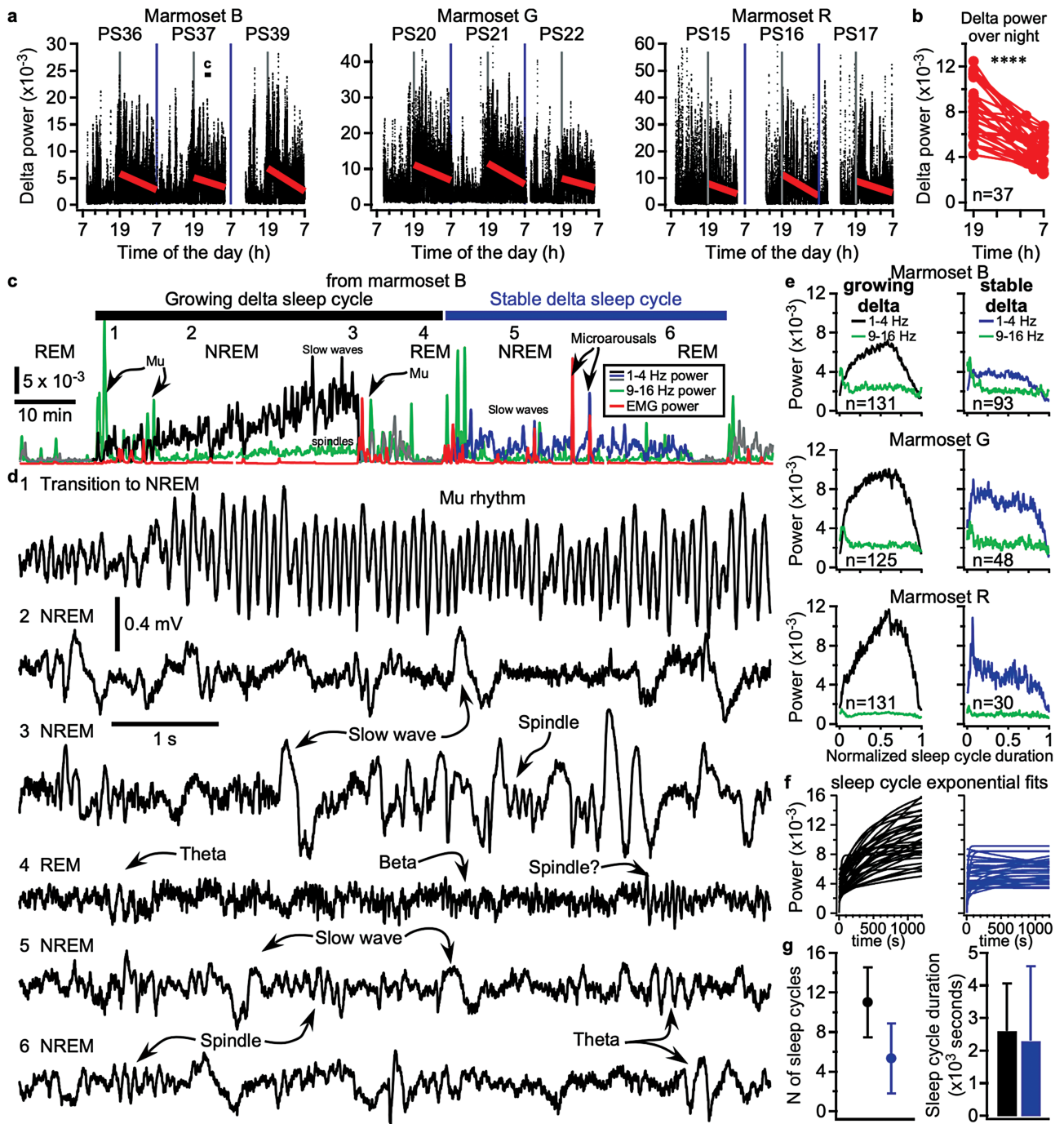
Figure 3. Dynamics of nocturnal delta power. (a) Examples of daily dynamics of delta power. Each panel shows 3 day–night recordings of each marmoset (B, G, R). Linear fitting of delta power during dark period is shown in red. (b) Linear fitting of delta power during dark period computed for 37 nights from 3 marmosets. Delta power at the beginning and end of the nights was compared with Wilcoxon matched-pairs signed rank test, $p < .0001$. (c) Examples of delta power, mu power and muscle power for 2 sleep cycles. (d1–d6) Examples of LFP recordings from somatosensory cortex corresponding to different states of sleep and indicated in (c). Averaged dynamics of delta power and mu power during sleep cycles with growing delta power and stable delta power for three animals. X-axis is normalized duration of NREM sleep period of each computed sleep cycle. (f) Each trace is an exponential fit of the averaged growing delta (left, black) or stable delta (right blue) sleep cycle over one night of recording. (g) Averaged number of sleep cycles as well as duration of sleep cycles with growing delta power (black) and stable delta power (blue).

sometimes interrupted with opening of eyes leading to waking states and proceeding to sleep at other times.

During behavioral drowsiness and naps, marmosets G and B preferred to stay next to each other in a hammock or in a little hut, while marmoset R seemed to play a role of a "guard",

staying awake next to them, or hanging on an external wall of the home cage.

During night sleep, most of the time all three marmosets entered their house, leaned to each other, and stayed under a blanket. They woke up before light on (Supplementary video 1).
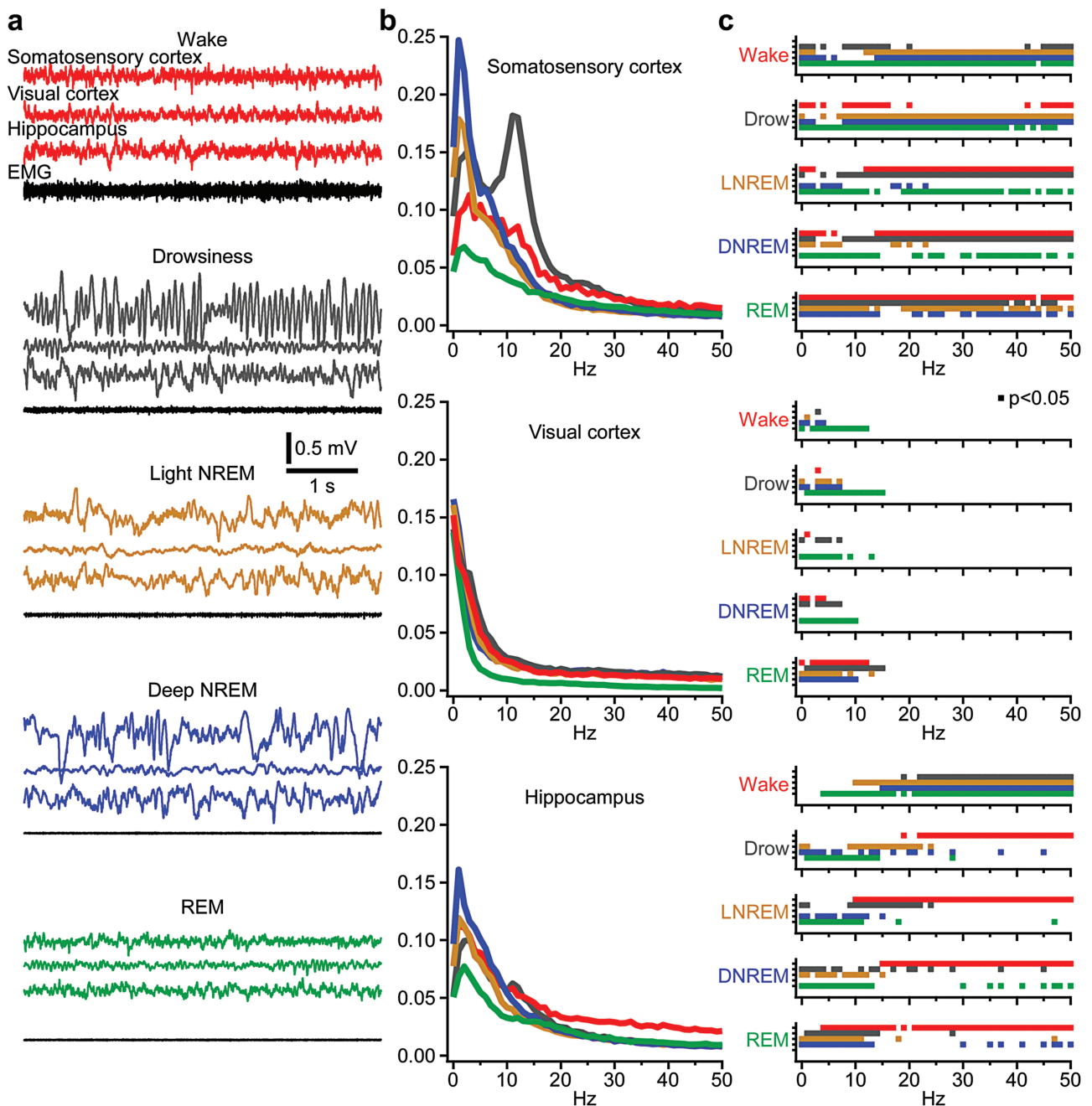
Figure 4. LFP power during five identified states. (a) Typical examples of somatosensory cortex, visual cortex and hippocampal CA1 LFP as well as nuchal EMG for five visually identified states. (b) Somatosensory (upper) visual (middle) and hippocampal (lower) averaged FFTs (10 segments from each animal) for each color-coded state. Note higher delta power during NREM sleep and higher mu power in somatosensory cortex during drowsiness. (c) Color-coded statistical difference for frequency bins with 1 Hz resolution of FFTs shown in panel b. $p < .05$ wo-way ANOVA with Tukey multiple comparison correction.

During visual inspection of day and night electrographic recordings from cortex, hippocampus and muscles in freely behaving common marmosets, we distinguished the following five brain states: wakefulness, drowsiness, light NREM, deep NREM, and REM sleep.

Electrophysiological recordings

LFP and EMG wireless recordings presented here were conducted 20–24 h/day, 3–5 days/week for about a month in 3 marmosets living together in the same home cage.

Waking state

During waking state, the LFP was either activated or displayed oscillatory activities in alpha, mu, and beta frequency ranges with occasional sharp-wave ripples in ventral hippocampal CA1 (Figure 1). Active wake was defined as periods with high amplitude neck muscle activities. Recordings during active movements were occasionally contaminated with movement artifacts in various frequency ranges (Figure 1a, b). They were considered as waking state and were not analyzed in detail. However, most of the recordings were artifact free. Alpha rhythm was more prominent in visual cortex and CA1 when muscle tone was
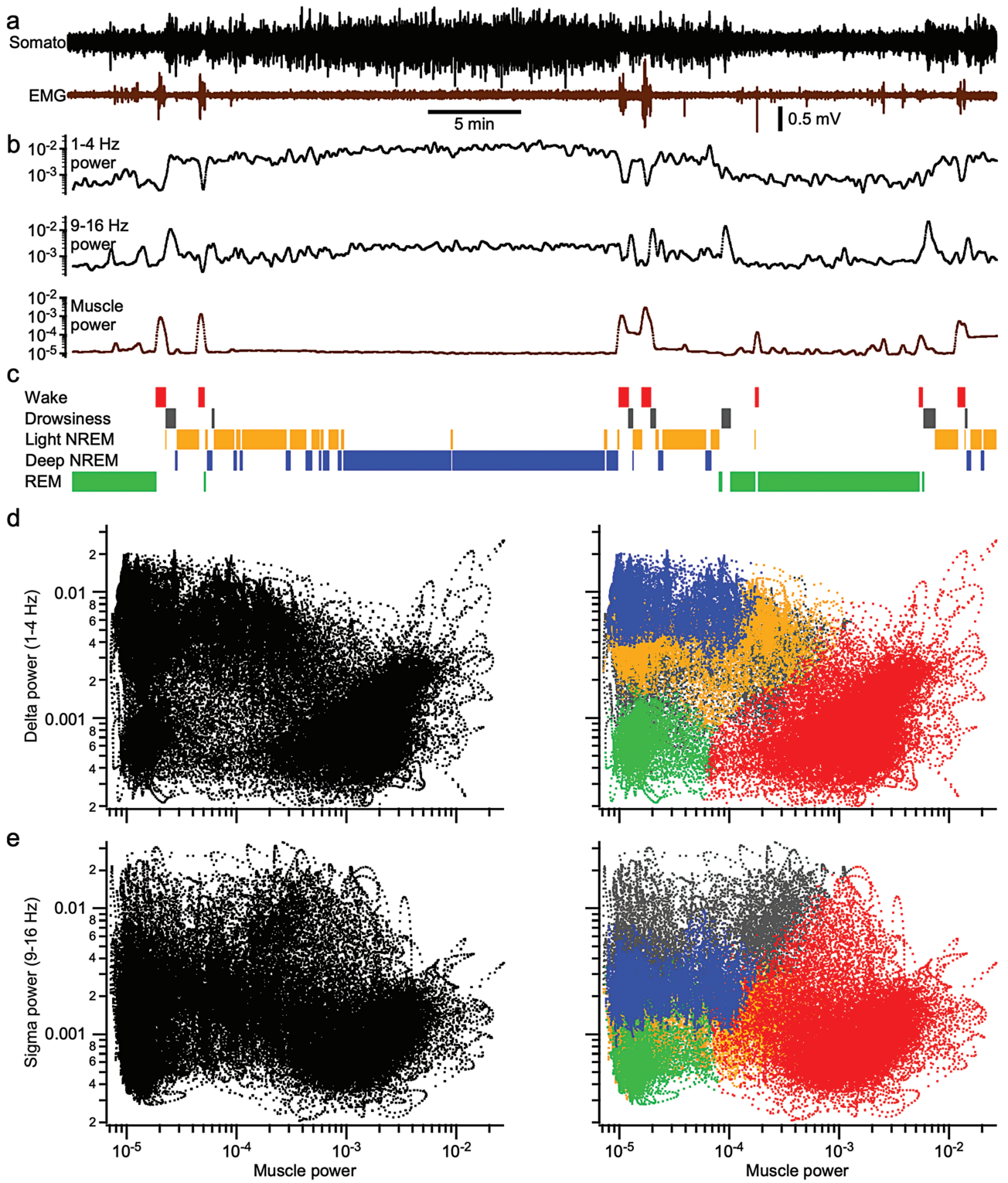
Figure 5. Automatic detection of brain states. **(a)** Original LFP recordings from somatosensory area with corresponding EMG. This segment includes all five states. **(b)** Dynamics of LFP power in delta and sigma bands and of muscle power corresponding to the recordings in panel a. Each point represents power value calculated in sliding 30 s windows with 29 s overlap centered around every time point (every second). **(c)** A result of automatically detected states of vigilance corresponding to panels a and b. **(d)** Scatter plots of delta vs. muscle power and **(e)** Scatter plots of sigma vs. muscle power. Each plot contains data from continuous 24 h recordings of one marmoset. Results of automatic detection of brain states are color coded. The color code is the same as in panel c.

low or stable (brighter colors under the red arrow in the middle panel of wavelet transform in Figure 1b). Prior to drowsiness, it often increased amplitude in centro-parietal and even frontal channels (Figure 1c).

Transitory mu-state (drowsiness)

We found a transitory state that was characterized with high-amplitude rhythmic activity (up to 1.5 mV) in the sigma range (9–16 Hz, with a peak in 11–13 Hz, Figure 1b, white arrow) that was particularly prominent in central areas of all animals and resembled human mu rhythm [38]. It was accompanied with marked transient reduction of alpha rhythm in visual and hippocampal electrodes in two out of three animals (Figure 1b, red arrow and c). During episodes of high-amplitude mu-rhythm, the animals did not move and had stable muscle tone (Figure 1a and d, Supplementary video 2). This brain state most often corresponded to drowsiness and could be observed between active wake episodes during daytime (Figure 1a and d). It was also common in transitions from wake or REM to NREM (Figure 2b, white arrow) or from NREM to REM sleep (Figure 3c, short spikes in sigma power in somatosensory and motor cortex). The amplitude of mu-rhythm in marmosets was often higher than that of slow waves and spindles during NREM sleep (Figure 3d). Depth-negative components of mu-rhythm oscillatory events were often accompanied with high-frequency ripples (Figure 1d).

NREM sleep stages

Neocortical LFP during NREM sleep (Figure 2) displayed slow waves, sleep spindles, events in the theta band and occasional ripples that could precede typical slow waves (Figure 2g) or occur during spindles. In agreement with previous observations [39–41], typical slow waves had depth-positive component characterized by virtual absence of fast oscillations followed by high amplitude depth-negative delta waves (HADNDW) accompanied with fast oscillations in beta, gamma or ripple frequency range (Figure 2a, b, c, f). However, different from other species in which we extensively recorded LFP (cats, mice), in marmosets, we observed HADNDW without preceding hyperpolarization (Figure 2c, g). HADNDW could also precede sleep spindles and be accompanied with neocortical ripples (Figure 2g).

In CA1 area of hippocampus (Figure 2e), we recorded sleep spindles and sharp-wave-ripple complexes or isolated ripples (Figure 2b–d).

We distinguished two stages of NREM sleep (see formal definition below). Both were characterized with the presence of slow waves and sleep spindles; however, deep NREM sleep differed from light NREM by higher levels of power in delta (1–4 Hz) and sigma (9–16 Hz) range (Figure 3d2, d3).

REM sleep

During REM, we observed activated cortical LFP with events in beta power band that were particularly prominent in visual and hippocampal electrodes (Figure 2b,g). The onset of REM LFP in hippocampus and visual cortex and lowering of muscle tone occurred earlier (typically 10–30 s) than the disappearing of slow oscillations in central areas (Figure 2a, b), where NREM sleep often terminated with high amplitude spindles (Figure 2b,)

or mu. In neocortical electrodes we observed occasional theta events composed of 3–5 cycles with frequency 7–9 Hz (Figure 3d4). In CA1 hippocampal recordings theta events were longer (5–10 cycles), but of low amplitude. Long REM could be interrupted with occasional spindles (Figures 2b and 3d4), short mu-rhythm events in motor and somatosensory areas (Figure 3c) or brief periods of wakefulness.

LFP power during different states

Based on visual definition of states we selected 10 segments of 30 s of each state (wake, drowsiness, light NREM, deep NREM, and REM) in each of the three marmosets and computed averaged fast Fourier transform (FFT) magnitude for neocortical (somatosensory and visual) and hippocampal CA1 electrodes (Figure 4). The power of all slow activities in all states was largest in somatosensory cortex, lower in CA1 and lowest in visual cortex (Figure 4b). Within somatosensory area, per Hertz analysis demonstrated that activities in frequency range 1–50 Hz were different in all states, with somewhat less different within the frequency range 5–15 Hz (Figure 4c). In visual cortex, the differences across states were found mainly in low frequency diapason (1–15 Hz) and they were not different between LNREM and DNREM (Figure 4c). In CA1, higher frequency activities (15–20 Hz and up) were different between wake and other states, but comparison to all other than wake states show the main differences were generally observed below 15 Hz (Figure 4c). Very strong power in frequency range of 8–16 Hz was seen in somatosensory and motor cortices during drowsiness. We did not observe any peak in theta frequency range neither in neocortex nor in CA1 hippocampus during REM sleep. This is not surprising, because similar to human observations [42] we saw only occasional theta events with just a few cycles interrupted by beta and occasional spindle oscillations (Figure 3d,4), but we never observed any sign of continuous theta oscillation commonly recorded from rodent hippocampus [11, 43]. An increase in broad beta/gamma activities compared to other states was recorded during wake in the somatosensory cortex and particularly hippocampus (Figure 4c). Apparently, it was not a reflection of muscle tone artifacts recorded with LFP/reference electrodes, because this kind of increase was absent in visual cortex.

Sleep cycles

During dark period, marmosets had multiple peaks of delta power that corresponded to NREM sleep (Figure 3a–c, see also Figure 7a). As expected, due to dynamics of sleep pressure, delta power was higher at the beginning of the night and decreased towards the morning (Figure 3a-b).

Periods between the beginning of transition to NREM sleep (increased delta power) and the end of the succeeding REM or wake (decreased delta power) were defined as individual sleep cycles (Figure 3c). There were between 16 and 20 sleep cycles per night.

Based on dynamics of delta power, we distinguished two types of sleep cycles—with progressively growing delta (Figure 3c, black trace, Figure 5a, b) and with relatively stable delta (Figure 3c, blue trace). The average peak of delta power values in "growing delta" sleep cycles was higher than in "stable delta" cycles (Figure 3c, e). Similar to human [44], cycles with growing

delta were seen all over the night, but the cycles with stable delta power never occurred in the first and second sleep cycle. NREM LFP during sleep cycles of both types displayed slow waves, sleep spindles and events in theta frequency band. Both types of sleep cycles usually began with a brief period of mu-like rhythm (Figure 3c, green trace) interrupted by short muscle twitches (Figure 3c, red trace). The mu rhythm peak at the beginning of sleep cycles was particularly prominent in two out of three marmosets (Figure 3e).

The "growing delta" cycles occurred more often than those with "stable delta" (387 vs. 171 out of 558 cycles analyzed, data from 3 animals), however, there was no significant difference in their duration (Figure 3g). Similar to a previous study [44], we used an exponential fit on the beginning portion (first 1200 s) of averaged growing and stable delta sleep cycle for each night analyzed (Figure 3f). For growing delta cycles, the fitting was good and it was achieved with 2–4 iterations, but for the vast majority of stable delta cycles the fitting did not follow an exponential function, therefore the extraction of Tau was meaningless. For asymptote level (Y_0 of exponential fit) we found that growing delta sleep cycle reach significantly higher power than for cycles with stable power (growing = 0.01329 ± 0.0064 vs. stable = 0.00652 ± 0.0029, $p < .0001$ Mann Whitney test).

Mu rhythm and spindles

Because mu activities and spindles occurred in the same frequency range (Figures 1–5), we investigated the distribution of several parameters of these activities hoping to obtain two clear peaks: one corresponding to spindles and another one corresponding to mu rhythm. We analyzed duration, frequency, and amplitude of detected events (Figure 6). The distribution partially overlapped for all measured parameters. The mu rhythm occurs during quiet wakefulness and, spindles occur during sleep. Therefore, we analyzed separately LFP activities in mu and spindle frequency range during quiet wakefulness/drowsiness and during light and deep sleep (Figure 6). The frequency of both types of events largely overlapped. However, there was a slight domination for spindles in a slower range (8–10 Hz, Figure 6, e), which corresponds to slow spindles. We previously discussed the possible mechanistic differences of fast and slow spindle origin [45] and the general conclusion of the discussed studies was that fast spindle properties fully correspond to the classical description of thalamic origin [46–50], while slow spindles may have other sources of generation. Similarity in the frequency of fast spindles and mu rhythm suggests that mu rhythm may share common mechanisms of generation with fast spindles. The maximal duration of 8–15 Hz oscillation during light NREM sleep was 2 s, during deep NREM sleep was 3 s, and it was over 10 s for quiet wakefulness (Figure 6e-g). Previously, spindles were defined as oscillations in the frequency range of 8–15 Hz, with maximal duration set arbitrarily to 3 s [51]. Most spindles that we detected had a duration of less than 1 s. Our analysis without any arbitrary set threshold identified 8–15 Hz events lasting up to 3 s as spindles, suggesting a high reliability of this analytical approach. During quiet wakefulness, there were many events in the same frequency range lasting between 1 and 10 s, occasionally up to 30 s. These events fully corresponded to the mu rhythm properties including behavioral correlates. The amplitude of 8–15 Hz events largely overlapped, except for the higher range, with a very small number detected during light NREM sleep and

a much larger number detected during quiet wakefulness. The slope of the linear fitting of duration vs. amplitude was low for spindles detected during sleep and it was much higher for mu rhythm recorded during quiet wakefulness (Figure 6, f). Almost all events exceeding 0.3 mV amplitude lasted longer than 3 s (Figure 6, f-g). Therefore, we conclude that most recorded mu rhythm events and spindles (fast spindles), show similar distribution for several parameters suggesting a common origin of these events. The main differences: they occur in different brain states (drowsiness vs. NREM sleep), longer and larger amplitude events were only happening during drowsiness. The majority of, if not all, events during drowsiness with a frequency of 8–15 Hz, high amplitude (above 0.3 mV) and long duration (more than 1 s) were likely mu rhythm events and not sleep spindles, because video recordings demonstrated that the animals were sitting with open eyes.

Formal definition and quantification of brain states

Overall, waking state in the absence of movement artifacts could be defined with high muscle tone and low amplitude LFP that resulted in low power in delta and sigma bands (Figure 4). Due to the absence of movements and the presence of high amplitude mu-like activity, the state of drowsiness was formally defined based on a moderate muscle tone and very high power in the sigma band (Figure 4). Presence of slow waves and spindles during light NREM (LNREM) sleep contributed to rise in delta and sigma power that was even higher in deep NREM (DNREM) sleep (Figure 4). Muscle tone during REM sleep was low and the LFP spectrum resembled that of a waking state (Figure 4).

These formal criteria were used as grounds for the development of procedure for automatic detection of brain states with the use of self-organizing maps described in Methods section (Figure 5). Six hours of recordings were manually scored by two independent experts and used as a "golden standard" (see Method section). The results of automatic classification were compared to the "golden standard" using two measures: the recall, which is the percentage of correctly identified "golden standard" states and the precision which is the percentage of automatically predicted states that corresponded to the "golden standard". Because there was disagreement between experts on the exact timing of transition between LNREM and DNREM, we validated precision of NREM detection as a whole, without separation on LNREM and DNREM. The recall/precision values were as follows (mean ± SD): wake 81.3 ± 9.7%/84.7 ± 13.5%; drowsiness 73.8 ± 4.9%/64.8 ± 15.9%; NREM sleep 93.5 ± 3.6%/94.5 ± 2.8%; REM sleep 90.0 ± 7.7%/88.6 ± 8.5%. The mean accuracy of the artificial neural networks that were trained separately for each marmoset was 90.4 ± 3.9%.

Day–night brain state dynamics

Marmosets are diurnal animals with 89.51 ± 9.61% of their total sleep (including LNREM, DNREM, and REM sleep) occurring during the dark phase (vs. 10.27 ± 9.63% during the light phase, $p < .0001$), unpaired t-test with Welch's correction. During light part of the day, marmosets were mostly awake (Figure 7), spending in this state on average 84.6 ± 8.1% of the time (vs. 14.9 ± 6.8% during dark phase, $p < .0001$). There were two peaks of activity between 7–10 a.m. and 2–4 p.m. Occasional episodes
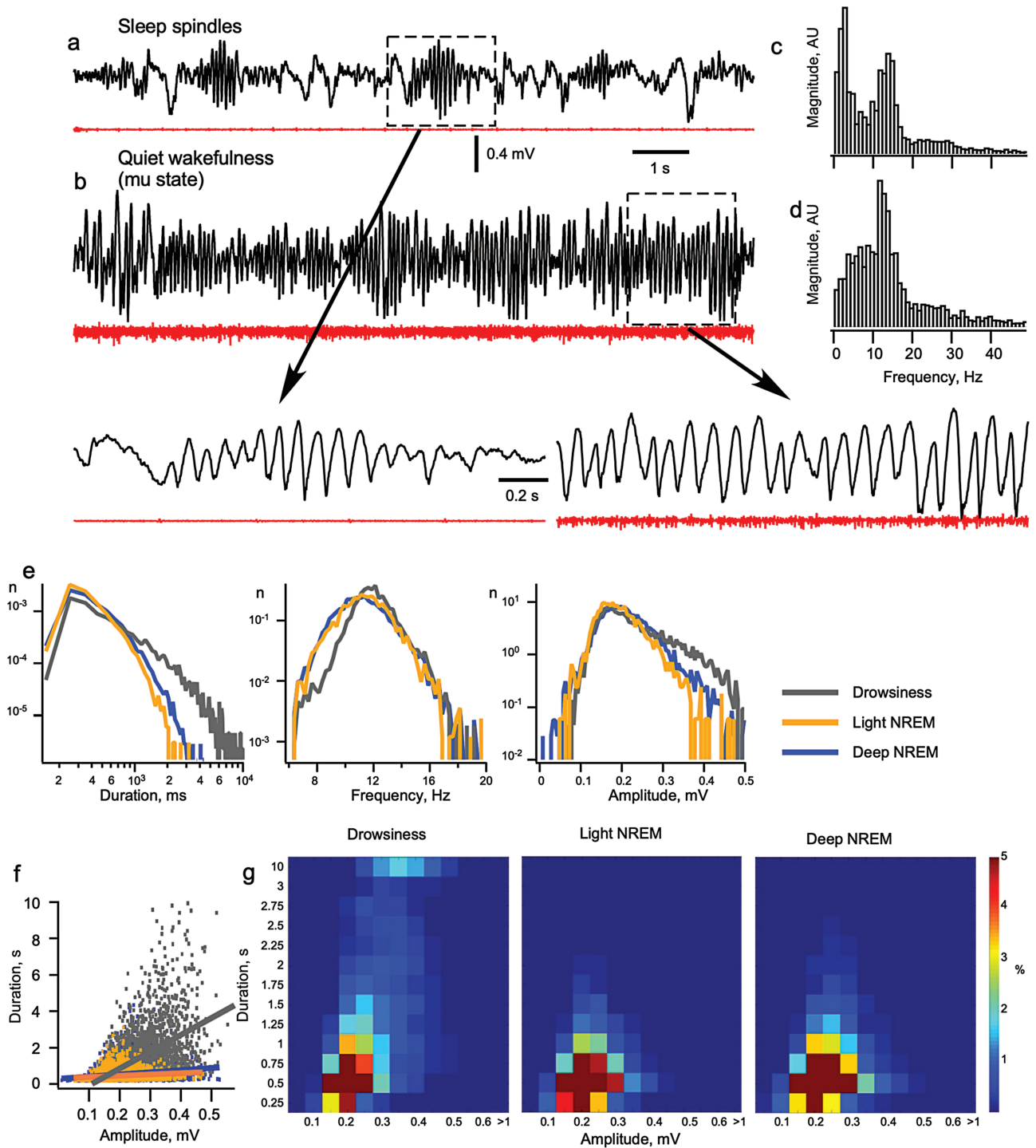
Figure 6. Basic properties of spindles and mu oscillations in somatosensory cortex. Examples of sleep LFP activity rich with spindles (a) and drowsiness state dominated by mu rhythm (b). (c) LFP power from segment shown in (a) and (d) LFP power from a segment shown in (b). Note the strong peak of power in 9–16 Hz range corresponding to spindles and mu rhythm. (d) Normalized distribution of duration, frequency, and amplitude of all events detected in a range 6–20 Hz in drowsiness, light and deep NREM sleep. Note overall similarity of distributions. However, longest and amplest events were recorded during drowsiness. (f) scatter plot and (g) color plot of relation of amplitude vs, duration of events in 6–20 Hz frequency range in drowsiness, light and deep NREM sleep.

of drowsiness (8.8 ± 6.6%) and naps occurred mostly between these hours. The naps were represented with DNREM (4.4 ± 3.3%) and less often with LNREM (1.7 ± 2.2%). Episodes of low muscle tone and activated LFP detected as REM took only 0.5 ± 0.6% of the light period.

Usually, marmosets fell asleep before the lights went off. The marmoset R, which was submissive (see behavioral observations) and had very little naps during the day went to sleep earlier than the two other marmosets (Figure 7b). They passed 14.2 ± 0.7% of nighttime in state of drowsiness (vs. 8.8 ± 6.6%
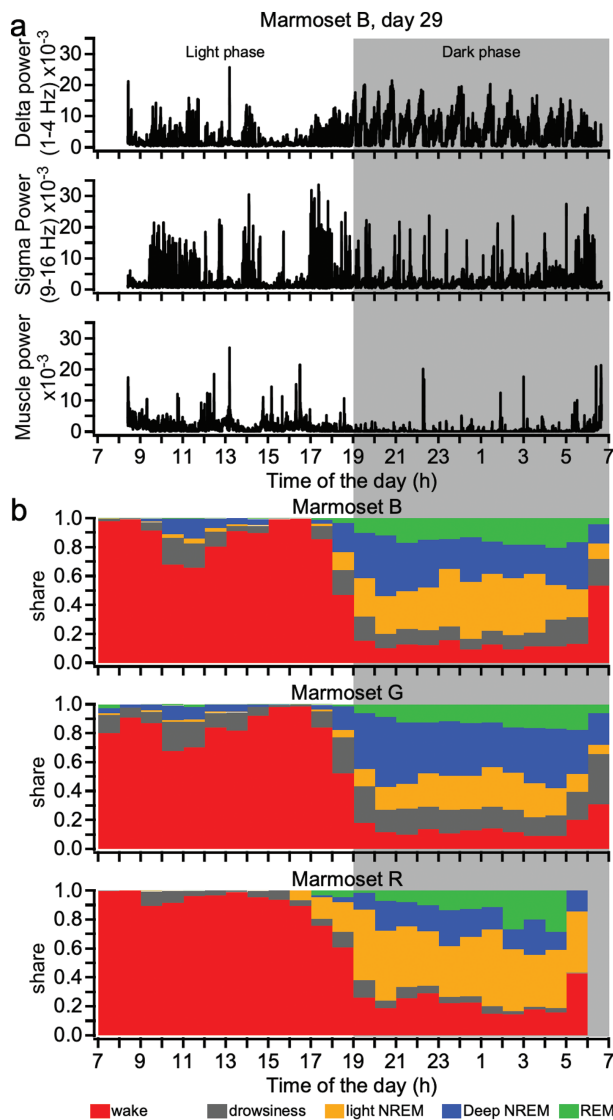
Figure 7. Day–night dynamics of brain states. (a) Example of delta, sigma, and muscle power dynamics over continuous day–night recording session of one marmoset. (b) Time share spent in each brain state averaged per hour for all investigated days shown separately for each marmoset (from top to bottom: marmosets B, G and R).

during day, $p < .0001$), that occurred mostly at the beginning and, for two out of three animals, also at the end of night (Figure 7). During the dark period, the marmosets spent on average $26.9 ± 10.1\%$ in LNREM and $30.9 ± 8.6\%$ in DNREM (vs. $1.7 ± 2.2\%$ for LNREM and $4.4 ± 3.3\%$ for DNREM during the light period, $p < .0001$ for both). In two animals, the proportion of DNREM was higher than that of LNREM in the first hours of the night. The share of REM sleep gradually increased closer to the morning time and took $13.1 ± 4\%$ over 12 h during the dark period. The marmosets spent $14.9 ± 6.8\%$ of the night in waking state, and its probability also increased toward morning. The marmosets typically woke up within the last hour of the dark phase (Figure 7).

The automatic method of brain state classification allowed detection of brain states of different length (Figure 8a). Most episodes were short, and as expected, the probability of long

episodes decreased with the episode duration. The number of transitions between the brain states of all types was higher at night than during the day (Figure 8a). Every day and night each animal had multiple short unstable brain states, particularly in transitory periods, and a few longer consolidated states.

There were differences in the duration of states depending on time of the day (Figure 8a, b). During daytime, there was a higher number of longer waking states, while episodes of all sleep types were shorter. At night, we did not observe long waking states. The number of night sleep episodes was higher than during daytime, and their duration was variable with mainly short states during usual daily naps and longer states at the end of the light cycle, when marmosets started to sleep (Figure 6b). There were only slight differences in episodes of drowsiness between day and night.

The majority of states formally detected as REM during light part of the day, were short (less than 10 s, Figure 8b, orange trace). Upon visual inspection, it was found that these periods of sudden lowering of the muscle tone were preceded and followed periods of active wake, and they were likely periods of quiet wakefulness, erroneously detected as REM.

Figure 5a–c demonstrates an example of recording at the beginning of the dark phase of light/dark cycle with multiple transitions between various short states at the beginning of a sleep cycle that were followed by more consolidated DNREM sleep, which also terminated with multiple short states in the transition to REM sleep at the end of the sleep cycle.

During a 24 h period, half of the waking time was spent in long consolidated states that had duration of 3000 s or longer. The duration of episodes that contributed to 50% of total time spent in drowsiness, LNREM, DNREM, and REM sleep were 36 s, 54 s, 86 s, and 166 s, correspondingly (Figure 8b).

These values reflect the level of consolidation of each brain state: wake and REM are more consolidated then both types of NREM, and as expected, the transitory state of drowsiness was the least stable.

For further analysis, we divided all sleep–wake episodes in three groups: "short" that took 10% of total brain state time, "medium" that occupied 10%–50% of time and "long" states that took top 50% of total brain state time (Figure 8b).

Transitions between brain states

We examined how the type and duration of each brain state could predict the type of the succeeding state (Figure 8c). Overall, waking episodes were more likely to terminate with drowsiness. Relatively brief wake could occur just before the beginning of unstable NREM sleep (Figure 5c) or could manifest as micro-arousals that only slightly affected the depth of ongoing sleep (Figure 5a). Long consolidated wake usually terminated with drowsiness. After long periods of active wake, we occasionally observed periods of activated LFP and very low muscle tone that could last up to tens of seconds. These recordings by their spectral characteristics or general shape of the LFP were undistinguishable from REM and therefore were detected as REM by automatic detection procedure. We also occasionally observed periods of increased muscle tone in the middle of long REM episodes that were detected as wake (Figure 5a,b).

Brain states with high mu activity of different duration could be followed by any state of vigilance, which confirms that this
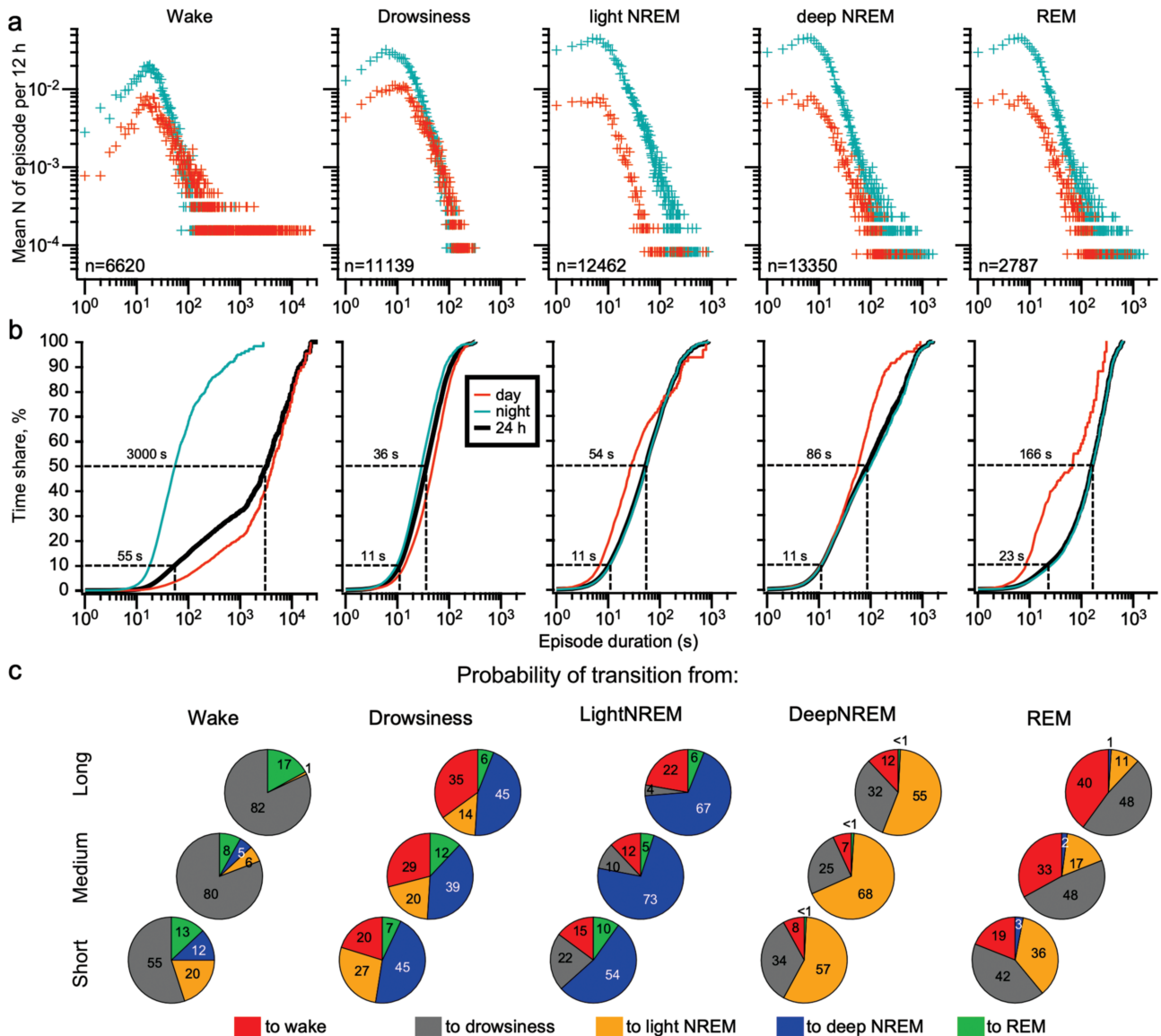
Figure 8. Duration of states and transition between states. **(a)** Mean number of wake, drowsiness, light NREM, deep NREM, and REM episodes with various duration during day (orange) and night (light blue) pooled from all automatically classified recordings from all marmosets and all days analyzed. (b) Time share of wake, drowsiness, LNREM, DNREM, and REM. Short episodes were all episodes with a time share 10% or less; long episodes were all episodes with a time share more than 50%. The data are shown separately for 24 h (black), day (orange) and night periods (blue). **(c)** Probability of transition to each type of brain state according to the preceding state and its duration (short, medium, or long).

brain state is a state of transition. Overall, it was more likely to proceed to NREM sleep, that is why we call this brain state as "drowsiness" (Supplementary video 3). Quite often, during falling asleep, the episodes of mu-like activity were interrupted by short wake with movements. The same type of activity could also be seen in transition from NREM to REM (Figure 5a–c).

Light NREM could also proceed to any brain state; however, most often it was followed by deep NREM.

Deep NREM was more likely to transition to light NREM with smaller chances to terminate with drowsiness or wake. It is worth noting that DNREM almost never was immediately followed by REM, as well as REM was almost never followed by DNREM. Transitions between deep sleep and REM occurred via LNREM or drowsiness, sometimes with short interruptions with wake (Figure 2b – white arrow).

Discussion

Major findings

We performed longitudinal wireless multi-channel LFP recordings from five neocortical areas and CA1 hippocampus in three marmosets living in the same cage allowing natural interactions between animals. Marmosets were mostly awake during light phase and sleeping during dark phase of light–dark cycle with 16–20 sleep cycles. Based on LFP patterns and spectral characteristics, we defined five different brain states.

(1) Wakefulness characterized by LFP activation/desynchronization or beta activity with variable muscle tone or alpha activity dominating occipital areas and stable muscle tone. In the hippocampus, we observed occasional sharp-wave ripples and during exploration we observed short groups but not continuous

theta waves. (2) Drowsiness characterized by high amplitude (about 1 mV) mu rhythm over somatosensory and motor cortex, and absence of movements. Mu rhythm was accompanied with neocortical ripples. (3) LNREM, characterized by slow waves and spindles of relatively low power. (4) DNREM, characterized by slow waves and spindles of relatively high power. The neck muscle tone was low and stable during both LNREM and DNREM, with occasionally higher tone during LNREM. Sharp-wave ripples were present in the hippocampus. (5) During REM sleep, LFPs recorded from frontal, motor and somatosensory cortices were desynchronized/activated, but in visual cortex and hippocampus, it was dominated by well-organized beta rhythm. In the hippocampus, we also recorded theta waves grouped in 3–5 wave cycles, but not continuous theta oscillation.

In agreement with sleep homeostasis theory [52, 53], the power of low frequency activities decreased from the beginning of night sleep till the end of the night sleep (Figure 3a-b). However, NREM periods within each individual sleep cycle were different. About two thirds of NREM periods were characterized by progressively increasing low frequency activities. Another third of NREM cycles was characterized by low and stable low frequency power (Figure 3). Such two types of sleep cycles were previously published in figures for rhesus monkeys [16, 54], but were not described or discussed in the text. This phenomenon was however described in human [55, 56]. The two dynamics observed within sleep cycles could depend on progressive involvement into delta activity of cortical neurons due to activation of neuromodulators [57] resulting from modulation of discharge rates of neurons within neuromodulatory systems [58, 59]. The duration of sleep cycles was roughly 30 min (Figure 3), which is 3–4 times shorter than in human [60], but is similar to a previous report [25]. What controls the duration of sleep cycles is unknown. It is likely that either sleep promoting or wake promoting hypothalamic/brainstem systems contribute [61]. In mice, manipulation of hypothalamic hypocretin neuron KCNQ2 channels mediating M-current dramatically modulated sleep fragmentation [62]. Therefore, it is likely that hypocretin expressing neurons control sleep cycle too. If that is true, species specific dynamics of M-current that depends on KCNQ2 channel density can be responsible for the duration of sleep cycle in different species. However, other cellular or network mechanisms controlling sleep cycle duration are possible too. The homeostatic time constant positively correlated to the weight of multiple nonprimate animal species, but in primates, including human it was higher than in other species (>16 h) almost independent of weight [63]. Although we did not do sleep deprivation experiments, it is reasonable to assume similar relations in marmosets.

Unexpected results

The most unexpected result of this study was finding an exceptionally powerful mu rhythm recorded over somatosensory and motor cortices. Since the initial description [64, 65], the mu rhythm is defined as a rhythm with dominant frequency 7–13 Hz, present over somatosensory and motor cortex which disappear upon movement. A current view is that mu rhythm plays a role in cognition [66], and mu rhythm desynchronization is correlated with several pathologies [67–69]. Although "*somatosensory wake alpha*" activities in marmosets were previously recorded with EEG [70], there was never mention of the strength of

this rhythm and its role in the transition between brain states. Here, we show the presence of regular high amplitude mu rhythm (10–14 Hz) in the state of drowsiness and in transition between different brain states, in particularly from wake or REM to NREM sleep. Mu rhythm organizes neocortical ripples, which appear around depth negative peaks (Figure 1). Beside its role in the generation of seizures [71, 72], neocortical ripples play a key role in memory retrieval [73].

The origin of mu rhythm is not well understood. There is a very strong correlation of somatosensory mu rhythm with BOLD signal in other brain regions, including multiple cortical areas, and subcortical structures such as thalamus, caudate nucleus, putamen, and hippocampus [74]. During quiet wakefulness the ventroposterior nucleus of thalamus generates rhythmic activities that are very similar to the cortical 14 Hz oscillations, and lesion of the same thalamic nucleus abolished cortical 14 Hz rhythm [75] suggesting a thalamic origin of the mu rhythm. However, cortical anodal (presumably excitatory) direct current stimulation resulted in mu rhythm desynchronization [76], suggesting that the cortex plays a very active role in mu rhythm generation. Thus, the mechanisms of mu rhythm generation seems to be similar to a recently described mechanisms of occipital alpha rhythm [77]. However, during wake, somatosensory mu and occipital alpha activities increase power in alternation (Figure 1), suggesting either difference in neuromodulatory control of somatosensory/motor system vs visual system, or pointing to a different mechanism. Because of the remarkable appearance of the mu rhythm in marmosets, future studies in these animals can reveal mechanisms underlying generation of this activity.

The second unexpected result is the absence of continuous theta rhythm in hippocampus during both wake exploration and REM sleep, commonly found in rodents [78]. Rather, REM LFP was characterized with events in low beta range resembling 20 Hz spindle-like wavelets described in other primates [16] with only occasional single waves in theta band. Continuous theta activity was also not reported in human [79], although direct hippocampal recordings from healthy human are absent.

The third unexpected result was a finding of HADNDW. We have long-lasting experience of recordings of cortical LFP from cats and mice during sleep [33, 40, 80–83], but in these species, we never observed waveforms similar to HADNDW and we did not see their description in the literature. HADNDW resembled depth negative components of sleep slow waves, but without preceding depth positive component. The fact that these waves are high amplitude and depth-negative suggests that they are mediated by synchronous excitation of a large groups of neurons. During typical slow wave, depth positive LFP components are associated with neuronal hyperpolarization and silence, while depth negativity is mediated by neuronal depolarization and occasional firing [84]. There are at least three major hypotheses that explain origin of depth negative LFP components associated with neuronal active states: (a) a release from neuronal slow afterhyperpolarization [85], (b) summation of spike-independent synaptic events (minis) [86], and (c) dynamical attractors mediated by feedback neural networks [87]. Because HADNDW are not preceded by depth positive wave (neuronal hyperpolarization) the hypothesis of release from afterhyperpolarization does not stand, the minis could definitely contribute to the onset of HADNDW, but it starts with already high neuronal activity the role of minis would be minimal.

Thus, dynamical attractors mediated by feedback networks is possibly the main mechanism mediating HADNDW. It is likely that cortical feedback networks are better developed in primates as compared to rodents or carnivores.

Relation to other marmoset studies

This study is possibly the first to obtain long-lasting, stable LFP intracortical recordings from freely behaving marmosets. Previous studies were using either ECoG or EEG recordings. Not surprising, similar to all previous studies on marmosets we observed that marmosets generally slept during night and were awake during day. In our study as well as in [26, 27, 29] the marmosets slept 12–13 h. Shorter [25] or longer [24] reported sleep durations could depend on the exact experimental conditions (duration of dawn, manipulation with recording system, keeping animals individually or in groups, etc.). We observed slightly higher number of sleep cycles and their shorter duration as compared to [25]. This could be explained by the fact that animals in [25] study were manipulated just prior to sleep and overall slept less, which could alter sleep pressure and thus affect the duration of sleep cycles. We obtained essentially similar data on the ratio of light and deep slow-wave sleep as in one of previous studies [25], but much less deep SWS was reported in [29]. This could be explained that in the cited study, the EEG recordings were done with closely located electrodes in bipolar configuration, and thus simultaneously occurring slow waves were just not picked up. We used multisite LFP recordings with reference in cerebellum, enabling detection of slow waves and thus deep sleep with a better resolution. Because we recorded LFPs from motor and somatosensory cortices we were able to identify very powerful mu rhythm during quiet wakefulness and in transition between any state, but more often to slow-wave sleep. Although we did not see this phenomenon being reported for marmosets, something similar was reported in tree shrew [88] and human [89].

The most widely used animals to study sleep are rodents, however their polyphasic sleep might not be the best for a translational study. A recent study in tree shrew showed that these animal display clear slow waves and spindles, that they display monophasic sleep (during dark) with multiple similarities to human sleep ([88]). However, they sleep more with multiple sleep bouts during light phase of dark–light cycle [90]. Thus, marmoset sleep appears to be a better model of human sleep–wake cycle.

Limitations

(1) In natural environment, common marmosets live in extended families (up to 15), they forage for food, hide/escape from predators, take care of youngsters, deal with changing weather conditions, etc. In our experiments, there were three male animals living in the same cage with standard temperature, humidity, 12 hours light/dark cycler, availability of food, absence of predators, etc. Therefore, the described sleep–wake patterns in conditions of wild-life could be different. However, even in the conditions of animal facilities, the marmosets developed some social structure, and there was one animal that checked environment while two others were having naps. Even more, relatively short duration of sleep cycles indicate that brain excitability was changing during sleep at relatively fast

rates, which is likely an adaptation for a life in wild environment allowing for relaxation during sleep, but still maintaining some level of awareness. (2) In our experiments, marmosets wore portable recording systems. We did not observe any sign of discomfort due to implanted devices, but still we cannot exclude that the presence of such devices affected their sleep wake pattern.

(3) The automatic procedure showed high levels of recall and precision in classifying NREM and REM sleep. However, it was not very accurate in the detection of drowsiness, because it was based on power calculated in 30 s windows which is typically used in clinic, while episodes of drowsiness rarely exceeded 10 s (Figure 6). Also, it was often difficult to distinguish between drowsiness and the beginning of light NREM (both manually and automatically). For the same reason, very short increasing in muscle tone and muscle twitches (less than half of the 30-s window size) could be missed by the automatic procedure. Overall, it would be important in future research to provide clear definition not based on arbitrary thresholds of difference between brain states vs. microstates. Based on such definition, it would be easy to define optimal window size for a state detection.

A few false positive detections of REM can be explained with brief episodes of muscle relaxation that sometimes followed active movements and therefore were scored as wake. However, these episodes were characterized with activated LFP and low muscle tone and thus formally corresponded to the definition of REM for automatic procedure. Therefore, it is yet unclear whether these episodes were periods of quiet wake with absence of muscle tone or episodes of true wake to REM transitions similar to what was observed in human infants [60]. At the same time, just as described in a previous study [25], during long REM sleep we observed episodes of increased muscle tone that on occasion could last tens of seconds and that did not allow us to automatically apply the rule that REM cannot follow wake. We chose to allow minor misclassifications of rare short episodes of unconventional changes of the muscle tone rather than missing long REM sleep.

Conclusion

The main objective of the study was to evaluate marmosets as an animal model closely matching human sleep. *Similar to human:* (1) marmosets are mainly awake during light period and asleep during dark period of light–dark cycle. (2) They have distinct light NREM sleep, deep sleep NREM, and REM sleep. (3) NREM sleep is characterized by spindle and slow wave activities, neocortical and hippocampal ripples. (4) Marmosets have clearly defined periodic sleep cycles. (5) Marmosets do not show continuous hippocampal theta rhythm. (6) During quiet wake, not accompanied by movements, marmosets display remarkable Mu rhythm. *Different from human:* (1) Spindles and slow waves are equally present during light and deep NREM sleep, although the power of these activities is smaller during light NREM as compared to deep NREM. (2) Sleep cycles of marmosets (~30 min) is much shorter than in adult human (~90 min) and even in human infants (50–60 min). Despite these small differences, we conclude that marmosets represent an excellent animal model to study human sleep. The observed differences in sleep–wake pattern between marmosets and human were quantitative but not qualitative.

Supplementary Material

Supplementary material is available at *SLEEP* online.

Disclosure Statement

None declared.

Data Availability

All data and codes used for analysis are available from the first (Olga Bukhtiyarova <olga.bukhtiyarova.1@ulaval.ca>) and corresponding (Igor Timofeev <Igor.Timofeev@fmed.ulaval.ca>) authors upon request.

References

1. Maquet P. The role of sleep in learning and memory. *Science*. 2001;**294**(5544):1048–1052. doi:10.1126/science.1062856.
2. Diekelmann S, *et al*. The memory function of sleep. *Nat Rev Neurosci*. 2010;**11**(2):114–126. doi:10.1038/nrn2762.
3. Rasch B, *et al*. About Sleep's role in memory. *Physiol Rev*. 2013;**93**(2):681–766. doi:10.1152/physrev.00032.2012.
4. Timofeev I, *et al*. Neocortical seizures: initiation, development and cessation. *Neuroscience*. 2004;**123**(2):299–336. doi:10.1016/j.neuroscience.2003.08.051.
5. Frauscher B, *et al*. Sleep, oscillations, interictal discharges, and seizures in human focal epilepsy. *Neurobiol Dis*. 2019;**127**:545–553. doi:10.1016/j.nbd.2019.04.007.
6. Ruckebusch Y; Gaujoux. Sleep patterns of the laboratory cat. *Electroencephalogr Clin Neurophysiol*. 1976;**41**(5):483–490. doi:10.1016/0013-4694(76)90060-2.
7. Kaitin KI, *et al*. Sleep fragmentation in canine narcolepsy. *Sleep* 1986;**9**(1):116–119. doi:10.1093/sleep/9.1.116.
8. Tobler I, *et al*. Altered circadian activity rhythms and sleep in mice devoid of prion protein. *Nature* 1996;**380**(6575):639–642. doi:10.1038/380639a0.
9. Tobler I, *et al*. Sleep and EEG slow-wave activity in the domestic cat: effect of sleep deprivation. *Behav Brain Res*. 1990;**37**(2):109–118. doi:10.1016/0166-4328(90)90086-t.
10. Marks GA, *et al*. A preliminary study of sleep in the ferret, Mustela putorius furo: a carnivore with an extremely high proportion of REM sleep. *Sleep* 1996;**19**(2):83–93. doi:10.1093/sleep/19.2.83.
11. Gervasoni D, *et al*. Global forebrain dynamics predict rat behavioral states and their transitions. *J Neurosci*. 2004;**24**(49):11137–11147. doi:10.1523/JNEUROSCI.3524-04.2004.
12. Grand L, *et al*. Long-term synchronized electrophysiological and behavioral wireless monitoring of freely moving animals. *J Neurosci Methods*. 2013;**212**(2):237–241. doi:10.1016/j.jneumeth.2012.10.008.
13. Fernandez LMJ, *et al*. Highly dynamic spatiotemporal organization of low-frequency activities during behavioral states in the mouse cerebral cortex. *Cereb Cortex*. 2017;**27**(12):5444–5462.
14. Reite ML, *et al*. Normal sleep patterns in Macaque Monkey. *Arch Neurol*. 1965;**12**(2):133–144. doi:10.1001/archneur.1965.00460260023003.
15. Bert J, *et al*. The sleep of the baboon, *Papio papio*, under natural conditions and in the laboratory. *Electroencephalogr Clin Neurophysiol*. 1975;**39**(6):657–662. doi:10.1016/0013-4694(75)90079-6.
16. Hsieh KC, *et al*. Sleep architecture in unrestrained rhesus monkeys (*Macaca mulatta*) synchronized to 24-hour light-dark cycles. *Sleep* 2008;**31**(9):1239–1250.
17. Rachalski A, *et al*. Sleep electroencephalographic characteristics of the Cynomolgus monkey measured by telemetry. *J Sleep Res*. 2014;**23**(6):619–627. doi:10.1111/jsr.12189.
18. Mattison JA, *et al*. An overview of nonhuman primates in aging research. *Exp Gerontol*. 2017;**94**:41–45. doi:10.1016/j.exger.2016.12.005.
19. Datson NA, *et al*. Development of the first marmoset-specific DNA microarray (EUMAMA): a new genetic tool for large-scale expression profiling in a non-human primate. *BMC Genomics*. 2007;**8**(1):190. doi:10.1186/1471-2164-8-190.
20. Mashiko H, *et al*. Comparative anatomy of marmoset and mouse cortex from genomic expression. *J Neurosci*. 2012;**32**(15):5039.
21. MacDougall M, *et al*. Optogenetic manipulation of neural circuits in awake marmosets. *J Neurophysiol*. 2016;**116**(3):1286–1294. doi:10.1152/jn.00197.2016.
22. Miller CT, *et al*. Marmosets: a neuroscientific model of human social behavior. *Neuron* 2016;**90**(2):219–233. doi:10.1016/j.neuron.2016.03.018.
23. Cléry JC, *et al*. Neural network of social interaction observation in marmosets. *eLife* 2021;**10**:e65012.
24. Sri Kantha S, *et al*. Sleep quantitation in common marmoset, cotton top tamarin and squirrel monkey by non-invasive actigraphy. *Comp Biochem Physiol A*. 2006;**144**(2):203–210. doi:10.1016/j.cbpa.2006.02.043.
25. Crofts HS, *et al*. Investigation of the sleep electrocorticogram of the common marmoset (*Callithrix jacchus*) using radiotelemetry. *Clin Neurophysiol*. 2001;**112**(12):2265–2273. doi:10.1016/s1388-2457(01)00699-x.
26. Verhave PS, *et al*. REM sleep behavior disorder in the marmoset MPTP model of early parkinson disease. *Sleep* 2011;**34**(8):1119–1125. doi:10.5665/SLEEP.1174.
27. Hoffmann K, *et al*. Remote long-term registrations of sleep-wake rhythms, core body temperature and activity in marmoset monkeys. *Behav Brain Res*. 2012;**235**(2):113–123. doi:10.1016/j.bbr.2012.07.033.
28. Gervais NJ, *et al*. The middle-aged ovariectomized marmoset (*Callithrix jacchus*) as a model of menopausal

symptoms: preliminary evidence. *Neuroscience* 2016;**337**:1–8. doi:10.1016/j.neuroscience.2016.08.056.

29. Ishikawa A, *et al*. Investigation of sleep–wake rhythm in non-human primates without restraint during data collection. *Exp Anim*. 2017;**66**(1):51–60. doi:10.1538/expanim.16-0073.

30. Buzsáki G, *et al*. The origin of extracellular fields and currents—EEG, ECoG, LFP and spikes. *Nat Rev Neurosci*. 2012;**13**(6):407–420.

31. Sheroziya M, *et al*. Global intracellular slow-wave dynamics of the thalamocortical system. *J Neurosci*. 2014;**34**(26):8875–8893. doi:10.1523/JNEUROSCI.4460-13.2014.

32. Durán E, *et al*. Sleep stage dynamics in neocortex and hippocampus. *Sleep*. 2018;**41**(6):1–11.

33. Soltani S, *et al*. Sleep–wake cycle in young and older mice. *Front Syst Neurosci*. 2019;**13**:51. doi:10.3389/fnsys.2019.00051.

34. Vyazovskiy VV, *et al*. Local sleep in awake rats. *Nature* 2011;**472**(7344):443–447. doi:10.1038/nature10009.

35. Funk Chadd M, *et al*. Local slow waves in superficial layers of primary cortical areas during REM sleep. *Curr Biol*. 2016;**26**(3):396–403.

36. Bernardi G, *et al*. Regional delta waves in human rapid eye movement sleep. *J Neurosci*. 2019;**39**(14):26862686.–268622697. doi:10.1523/jneurosci.2298-18.2019.

37. Paxinos G, Watson C, Petrides M, Rosa M, Tokuno H. *The marmoset brain in stereotaxic coordinates*. 1st ed. Academic Press/Elsevier; 2012.

38. Niedermeyer E. Alpha rhythms as physiological and abnormal phenomena. *Int J Psychophysiol*. 1997;**26**(1):31–49. doi:10.1016/s0167-8760(97)00754-x.

39. Bukhtiyarova O, *et al*. Slow wave detection in sleeping mice: comparison of traditional and machine learning methods. *J Neurosci Methods*. 2019;**316**:35–45. doi:10.1016/j.jneumeth.2018.08.016.

40. Chauvette S, *et al*. Properties of slow oscillation during slow-wave sleep and anesthesia in cats. *J Neurosci*. 2011;**31**(42):14998–15008. doi:10.1523/JNEUROSCI.2339-11.2011.

41. Mukovski M, *et al*. Detection of active and silent states in neocortical neurons from the field potential signal during slow-wave sleep. *Cereb Cortex*. 2007;**17**(2):400–414. doi:10.1093/cercor/bhj157.

42. Cantero JL, *et al*. Sleep-Dependent θ oscillations in the human hippocampus and neocortex. *J Neurosci*. 2003;**23**(34):10897–10903. doi:10.1523/jneurosci.23-34-10897.2003.

43. Grosmark AD, *et al*. REM sleep reorganizes hippocampal excitability. *Neuron* 2012;**75**(6):1001–1007. doi:10.1016/j.neuron.2012.08.015.

44. Trachsel L, *et al*. Effect of sleep deprivation on EEG slow wave activity within non-REM sleep episodes in the rat. *Electroencephalogr Clin Neurophysiol*. 1989;**73**(2):167–171. doi:10.1016/0013-4694(89)90197-1.

45. Timofeev I, *et al*. The spindles: are they still thalamic? *Sleep* 2013;**36**(6):825–826. doi:10.5665/sleep.2702.

46. Morison RS, *et al*. Electrical activity of the thalamus and basal ganglia in decorticate cats. *J Neurophysiol*. 1945;**8**:309–314.

47. Morison RS, *et al*. A study of thalamo-cortical relations. *Am J Physiol*. 1942;**135**:281–292.

48. Steriade M, *et al*. Thalamocortical oscillations in the sleeping and aroused brain. *Science* 1993;**262**(5134):679–685. doi:10.1126/science.8235588.

49. von Krosigk M, *et al*. Cellular mechanisms of a synchronized oscillation in the thalamus. *Science* 1993;**261**(5119):361–364. doi:10.1126/science.8392750.

50. Timofeev I, *et al*. Low-frequency rhythms in the thalamus of intact-cortex and decorticated cats. *J Neurophysiol*. 1996;**76**(6):4152–4168. doi:10.1152/jn.1996.76.6.4152.

51. Mölle M, *et al*. Fast and slow spindles during the sleep slow oscillation: disparate coalescence and engagement in memory processing. *Sleep* 2011;**34**(10):1411–1421. doi:10.5665/SLEEP.1290.

52. Borbely AA, *et al*. A two process model of sleep regulation. *Hum Neurobiol*. 1982;**1**(3):195–204.

53. Achermann P, *et al*. Mathematical models of sleep regulation. *Front Biosci*. 2003;**8**:s683–s693. doi:10.2741/1064.

54. Xu W, *et al*. Sequential neural activity in primary motor cortex during sleep. *J Neurosci*. 2019;**39**(19):36983698.–369833712. doi:10.1523/jneurosci.1408-18.2019.

55. Achermann P, *et al*. A model of human sleep homeostasis based on EEG slow-wave activity: quantitative comparison of data and simulations. *Brain Res Bull*. 1993;**31**(1-2):97–113. doi:10.1016/0361-9230(93)90016-5.

56. Borbely AA, *et al*. Sleep deprivation: effect on sleep stages and EEG power density in man. *Electroencephalogr Clin Neurophysiol*. 1981;**51**(5):483–495. doi:10.1016/0013-4694(81)90225-x.

57. Lee S-H, *et al*. Neuromodulation of brain states. *Neuron* 2012;**76**(1):209–222. doi:10.1016/j.neuron.2012.09.012.

58. Hassani OK, *et al*. Discharge profiles of identified GABAergic in comparison to cholinergic and putative glutamatergic basal forebrain neurons across the sleep-wake cycle. *J Neurosci*. 2009;**29**(38):11828–11840. doi:10.1523/JNEUROSCI.1259-09.2009.

59. Boucetta S, *et al*. Discharge profiles across the sleep–waking cycle of identified cholinergic, GABAergic, and glutamatergic neurons in the pontomesencephalic tegmentum of the rat. *J Neurosci*. 2014;**34**(13):4708–4727. doi:10.1523/JNEUROSCI.2617-13.2014.

60. Carskadon MA, Dement WC. *Chapter 2 - normal human sleep: an overview*. In: Kryger M, Roth T, Dement WC, eds. *Principles and Practice of Sleep Medicine*. 6th ed. Elsevier; 2017: 15–24.e13.

61. Scammell TE, *et al*. Neural circuitry of wakefulness and sleep. *Neuron*. 2017;**93**(4):747–765. doi:10.1016/j.neuron.2017.01.014.

62. Li S-B, *et al*. Hyperexcitable arousal circuits drive sleep instability during aging. *Science* 2022;**375**(6583):eabh3021.

63. Phillips AJK, *et al*. Mammalian sleep dynamics: how diverse features arise from a common physiological framework. *PLoS Comput Biol*. 2010;**6**(6):e1000826. doi:10.1371/journal.pcbi.1000826.

64. Gastaut H. Etude electrocorticographique de la reactivite des rythmes rolandiques. *Rev Neurol (Paris)*. 1952;**87**(2):176–182.

65. Gastaut H, *et al*. Etude d'une activite electroencephalographique meconnue: le rythme rolandique en arceau. *Mars Med*. 1952;**89**(6):296–310.

66. Hobson HM, *et al*. The interpretation of mu suppression as an index of mirror neuron activity: past, present and future. *R Soc Open Sci*. 2017;**4**(3):160662. doi:10.1098/rsos.160662.

67. Derambure P, *et al*. Abnormal cortical activation during planning of voluntary movement in patients with epilepsy with focal motor seizures: event-related desynchronization study of electroencephalographic mu rhythm. *Epilepsia* 1997;**38**(6):655–662. doi:10.1111/j.1528-1157.1997.tb01234.x.

68. Oberman LM, *et al*. EEG evidence for mirror neuron dysfunction in autism spectrum disorders. *Cogn Brain Res*. 2005;**24**(2):190–198.

69. Heida T, *et al*. Event-related mu-rhythm desynchronization during movement observation is impaired in Parkinson's disease. *Clin Neurophysiol*. 2014;**125**(9):1819–1825.

70. Philippens IH, et al. Neurofeedback training on sensorimotor rhythm in marmoset monkeys. *Neuroreport* 2010;**21**(5):328–332. doi:10.1097/WNR.0b013e3283360ba8.

71. Grenier F, et al. Neocortical very fast oscillations (ripples, 80–200 Hz) during seizures: intracellular correlates. *J Neurophysiol*. 2003;**89**(2):841–852. doi:10.1152/jn.00420.2002.

72. Jefferys JG, et al. Mechanisms of physiological and epileptic HFO generation. *Prog Neurobiol*. 2012;**98**(3):250–264. doi:10.1016/j.pneurobio.2012.02.005.

73. Vaz AP, et al. Coupled ripple oscillations between the medial temporal lobe and neocortex retrieve human memory. *Science* 2019;**363**(6430):975–978. doi:10.1126/science.aau8956.

74. Yin S, et al. Amplitude of sensorimotor mu rhythm is correlated with BOLD from multiple brain regions: a simultaneous EEG-fMRI study. *Front Hum Neurosci*. 2016;**10**(364):364. doi:10.3389/fnhum.2016.00364.

75. Bouyer JJ, et al. Thalamic rhythms in cat during quiet wakefulness and immobility. *Electroencephalogr Clin Neurophysiol*. 1983;**55**(2):180–187. doi:10.1016/0013-4694(83)90186-4.

76. Matsumoto J, et al. Modulation of mu rhythm desynchronization during motor imagery by transcranial direct current stimulation. *J Neuroeng Rehabil*. 2010;**7**(1):27. doi:10.1186/1743-0003-7-27.

77. Nestvogel DB, et al. Visual thalamocortical mechanisms of waking state-dependent activity and alpha oscillations. *Neuron* 2022;**110**(1):120–138.e124.

78. Buzsáki G, et al. Memory, navigation and theta rhythm in the hippocampal-entorhinal system. *Nat Neurosci*. 2013;**16**(2):130–138. doi:10.1038/nn.3304.

79. Iber C, Ancoli-Israel S, Chesson A, Quan S. *Manual for the Scoring of Sleep and Associated Events: Rules, Terminology and Technical Specifications*. Westchester: American Academy of Sleep Medicine; 2007.

80. Timofeev I, et al. Impact of intrinsic properties and synaptic factors on the activity of neocortical networks in vivo. *J Physiol (Paris)*. 2000;**94**(5-6):343–355.

81. Timofeev I, et al. Disfacilitation and active inhibition in the neocortex during the natural sleep-wake cycle: an intracellular study. *Proc Natl Acad Sci USA*. 2001;**98**(4):1924–1929. doi:10.1073/pnas.98.4.1924.

82. Steriade M, et al. Natural waking and sleep states: a view from inside neocortical neurons. *J Neurophysiol*. 2001;**85**(5):1969–1985. doi:10.1152/jn.2001.85.5.1969.

83. Chauvette S, et al. Origin of active states in local neocortical networks during slow sleep oscillation. *Cereb Cortex*. 2010;**20**:2660–2674. doi:10.1093/cercor/bhq009.

84. Contreras D, et al. Cellular basis of EEG slow rhythms: a study of dynamic corticothalamic relationships. *J Neurosci*. 1995;**15**(1):604–622.

85. Sanchez-Vives MV, et al. Cellular and network mechanisms of rhythmic recurrent activity in neocortex. *Nat Neurosci*. 2000;**3**(10):1027–1034. doi:10.1038/79848.

86. Timofeev I, et al. Origin of slow cortical oscillations in deafferented cortical slabs. *Cereb Cortex*. 2000;**10**(12):1185–1199. doi:10.1093/cercor/10.12.1185.

87. Cossart R, et al. Attractor dynamics of network UP states in the neocortex. *Nature* 2003;**423**(6937):283–288. doi:10.1038/nature01614.

88. Dimanico MM, et al. Aspects of tree shrew consolidated sleep structure resemble human sleep. *Commun Biol*. 2021;**4**(1):722. doi:10.1038/s42003-021-02234-7.

89. Krishnan GP, et al. Cellular and neurochemical basis of sleep stages in the thalamocortical network. *eLife* 2016;**5**:e18607.

90. Coolen A, et al. Telemetric study of sleep architecture and sleep homeostasis in the day-active tree shrew *Tupaia belangeri*. *Sleep* 2012;**35**(6):879–888. doi:10.5665/sleep.1894.